POAC'23
Glasgow, UK

Proceedings of the 27th International Conference on
Port and Ocean Engineering under Arctic Conditions
June 12-14, Glasgow, UK

Evolution of Contact Area and Pressure during Ice Rubble Block-Block Interactions

Pritom Chakraborty[1], Rocky Taylor[1]
[1]Faculty of Engineering and Applied Science, Memorial University of Newfoundland, St. John's, NL Canada

ABSTRACT

Ice ridges pose potential risks to offshore, coastal and subsea infrastructure in ice prone regions. Ice rubble blocks in the keels of such ridges can rearrange and locally fail when external forces are applied, which can influence the associated contact areas and pressures that develop between blocks. This ultimately influences the freeze-bonding process between blocks which is a significant contributor to the development of overall ridge keel strength. Recent research has helped advance the understanding and modelling of freeze-bond strength as a function of in-situ conditions such as confinement, loading rate and submergence time. The implementation of such bond strength models in numerical simulations, such as those based on the discrete element method, requires representative estimates of block-block contact areas and pressures that develop for different levels of confining pressure. These contact areas and pressures are in turn governed by local ice failure processes between rubble blocks, which are influenced by block shape, orientation and indentation rate. In this paper, preliminary results are presented from an initial set of experiments conducted for ice blocks characterized by three different ice block orientation angles (30°, 45° and 60°) and for three indentation rates (0.5 mm/s, 0.25 mm/s, and 0.01 mm/s). In addition to load and displacement measurements, tactile sensors were used to capture area evolution and pressure distribution at the contact interface to help improve understanding of how actual contact geometries evolve as compared with idealized geometric intersection models based on nominal block shape. Corresponding video data from these tests also provide insights into the role spalling and crushing play in the observed contact area and pressure evolution at the interface between blocks. Based on preliminary results for the range of conditions considered, the dependence on block orientation for contact area evolution appears to be less sensitive than the dependence on indentaion rate.

KEY WORDS: Ice mechanics; Ice rubble block; Ice rubble block-block interactions; Contact area evolution; Freeze bonds;

NOMENCLATURE

t	Ice Thickness
δ	Penetration depth
θ	Orientation Angle
A_{actual}	Actual Contact Area
$A_{nominal}$	Nominal Contact Area
ψ_{AC}	Contact Area Correction Factor

INTRODUCTION

In the Arctic region, ice ridges pose a hazard for the arctic marine pipelines and subsea systems (Palmer & Croasdale, 2013). A compression ice ridge is formed when two ice sheets collide into each other. This compression or collision between the ice sheets results in the formation of sail, keel, and consolidated layer, shown in Fig. 1 (a) (Jensen et al., 2001). The sail and keel feature of a ridge is comprised of ice rubble blocks which are formed due of the crushing and flexural failure of the ice sheets in the compression process (Heinonen, 2004).

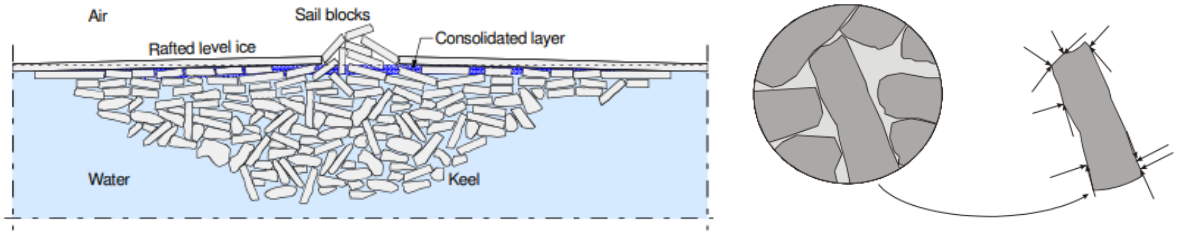

(a) (b)

Figure 1. (a) Cross-section sketch of an ice ridge (Jensen et al., 2001) and (b) Contact force between adjacent ice blocks in keels (Heinonen, 2004)

The partially consolidated ice rubble blocks are arranged in random orientations in the keel. When the keel encounters an external compressive load due to a marine pipeline or subsea structure, the ice rubble blocks get re-oriented (Bailey et al., 2015). The external forces are transmitted via the contact forces (normal and tangential) between the ice rubble blocks as shown in Fig. 1 (b) (Heinonen, 2004). When the ice rubble blocks are compressed, freeze-bonds between the blocks at the contact interface are put under stress, resulting in the breakage of some freeze bonds. This failure initiates the change in the geometric configuration of the rubble (Afzali, 2021). The primary objective of this study is to observe the change in the geometric structure of the contact interface of two ice rubble blocks that have undergone compressive failure process.

Numerical simulations, such as discrete element modelling utilized by Alfazi et al. (2021), have been performed to model and study the failure behaviour of the ice rubble and the breakage of freeze bonds between the ice rubble blocks. This experimental program seeks primarily to investigate the contact area at the intersection of two ice rubble blocks. Through these tests investigations are made into the effects of block orientation and indentation rates on the contact areas and pressures evolution during local ice failure processes. This paper introduces a contact area correction factor (ψ_{AC}) as a ratio of the actual (or experimental) contact area to the nominal (or theoretical) contact area where the nominal contact area is the geometric area of the surface in contact and the actual contact area is the area of contact between two surfaces in contact under load. The nominal contact area is determined from the geometric intersection area of two blocks whereas the actual contact area is determined from the experiment using a tactile sensor between the ice blocks. The contact area correction factor is a function of the penetration depth. The factor is used to examine the deformation at the contact surface and adjust for the difference between the actual and nominal contact area. Alfazi et al. (2021) used a similar contact area factor (c_f) in their study to account for the difference between the estimated freeze bond strength and the actual freeze bond strength by adjusting the estimated DEM freeze bond strength value to a more accurate value. The main difference in the present experiments is that the contact area correction factor is used to

estimate the contact area evolution at the block-block interface during crushing failure whereas Alfazi et al. (2021) applied the correction factor to estimate the contact pressure between blocks due to hydrostatic pressure. In these tests, the effects of changes in indentation rates and ice block orientation on contact area evolution were also examined. In the present paper, for the orientation of the ice blocks, rotation along a single axes is considered. Multiple axes of rotations or compound angle block geometry will be considered in a future study.

EXPERIMENTAL SETUP AND DESIGN

For the preparation of ice specimens, ice blocks of 7”x5”x4” (177.8 mm x 127 mm x 101.6 mm) were fabricated by crushing freshwater, polycrystalline ice into ice seeds using an industrial ice crushing machine then freezing the ice seeds with chilled water. The cooled water and ice seeds were compacted in a mold and placed into the freezer at -13°C. Following one day of freezing, the ice blocks were shaped to the desired profiles using a bandsaw. As illustrated in Figure 2 (a), (b) & (c), the ice specimens with three different orientation angles were considered: 30°, 45° and 60°. The average thickness of all these ice specimens were kept at 4” (101.6 mm). After the shaping, individual specimens were placed in separate circular specimen holders with average inner diameter (I.D.) of 11.5” (292.1 mm). The shaped specimens were placed in the center of the specimen holder and the empty space around the specimen was filled with seed ice and cooled water. Wooden planks were placed around the four sides of the ice specimen to ensure the specimen did not shift horizontally. Prior to testing, prepared ice specimens were stored at -13°C for 16-24 hours to ensure that the internal temperature of the ice specimens reached approximately -13°C. Additionally, a soil box of dimension 11”x11”x2” (279.4 mm x 279.4 mm x 50.8 mm) was used to grow a flat plate of ice with the similar fabrication process of the ice specimens.

Tests were conducted using the Materials Testing System (MTS) machine, as shown in Figure 3, housed in the cold room facilities at the Memorial University of Newfoundland. During a test, the sample was mounted on to the MTS Load Frame by tightly affixing the specimen holder on to the carriage. At the bottom, the soil box containing the flat ice surface is tightly attached to the vertical hydraulic ram and positioned such that the ice surface would make contact at the direct edge of the ice specimen. A tactile pressure sensor was placed on the top of the flat ice surface directly below edge of the ice specimen as shown in Figure 4.

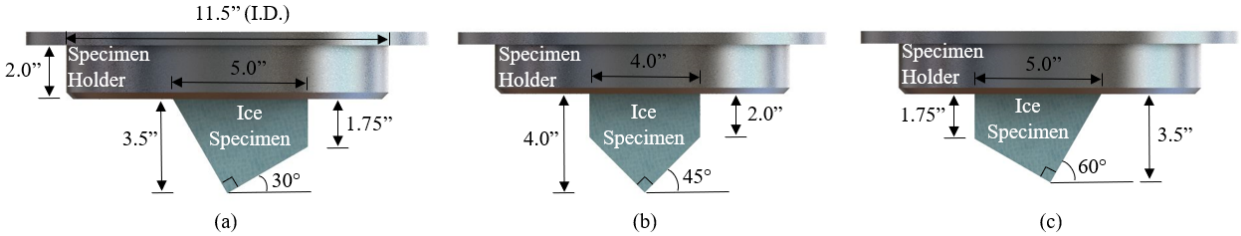

Figure 2. CAD Drawings of ice blocks oriented at (a) 30° angle; (b) 45° angle; (c) 60° angle.

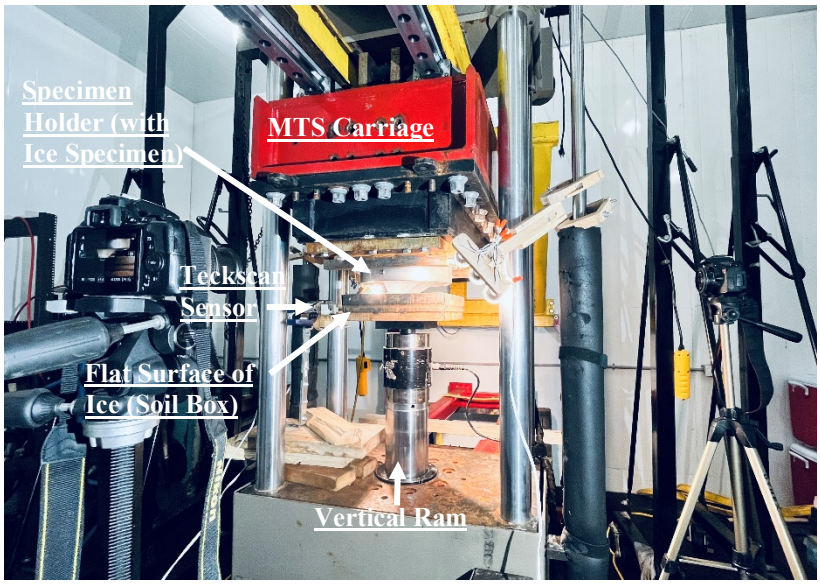

Figure 3. MTS Load Frame

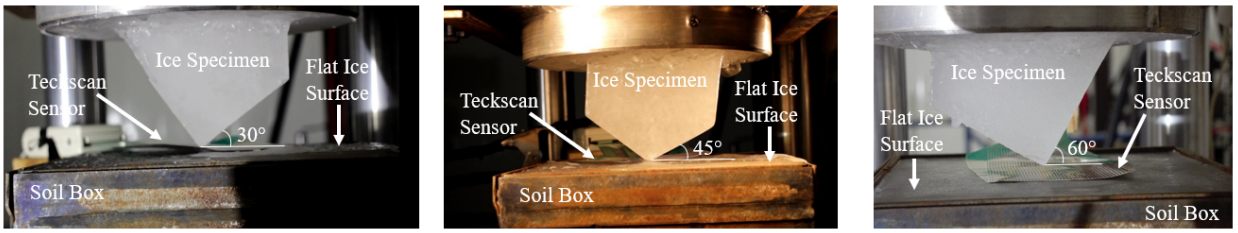

Figure 4. Arrangements of the ice specimen, Tekscan sensor and flat ice surface with MTS load frame

To investigate the contact area evolution of these ice tests, the load cell data from the MTS, video data, area and pressure distribution recordings from tactile sensor were synchronized and compared across the relevant timeframe to confirm crushing failure. It is important to highlight that determining the contact area of the ice specimen at the interface is an intricate process for a test as it can vary with displacement and with the erratic localized spalling events that occur during the experiment. For this reason, idealized geometric intersection models based on nominal block shape were considered as a starting point, assuming no spalling occurs during each test, for the purposes of analysis.

In order to estimate the contact area correction factor, the nominal (or theoritical) contact area must be calculated from the geometric intersection of ice rubble blocks oriented at a certain angle. The nominal contact area of the ice rubble block was calculated as a function of the penetration depth,

$$A_{nominal} = t\delta(tan\,\theta + cot\,\theta)\ [\text{mm}^2] \quad (1)$$

where δ is the penetration depth, t is the thickness of ice, and θ is the ice block orientation angle. For all the tests, ice thickness t value of 4" or 101.6 mm was used.

The contact area correction factor, ψ_{AC}, was calculated as a ratio of the actual contact area and the nominal contact area,

$$\psi_{AC} = \frac{A_{actual}}{A_{nominal}} \quad (2)$$

where A_{actual} is the actual contact area obtained from the tactile sensor data.

RESULTS AND DISCUSSION

A total of 8 experiments were completed for this study including repetitions. Three indentation rates and three block orientations were considered for this series of experiments. Of these 8 total tests, 2 tests were performed with an indentation rate of 0.25 mm/s and 0.5 mm/s for ice blocks oriented at 30° angle. Two tests were conducted at an indentation rate of 0.25 mm/s and 0.5 mm/s for ice blocks oriented at 60° angle. Two additional tests were completed for ice blocks oriented at 45° angle where both tests were performed at an indentation rate of 0.25 mm/s. Finally, two tests were performed at an indentation rate of 0.01 mm/s. The test matrix for the experimental program without repetitions is given in Table 1. The tests numbered 01-05 are categorized as fast tests, while Test 06 is categorized as a slow test.

Table 1. Test Matrix

Test No.	Test ID	Indentation Rate (mm/s)	Orientation (°)	Test Type
01	T01 _0p25_x30	0.25	30	Fast
02	T02 _0p5_x30	0.5	30	Fast
03	T03 _0p25_x60	0.25	60	Fast
04	T04 _0p5_x60	0.5	60	Fast
05	T05 _0p25_x45	0.25	45	Fast
06	T06 _0p01_x60	0.01	60	Slow

Influence of Indentation Rate

Testing was completed at three different indentation rates to provide a preliminary investigation of the effects of indentation rate on contact area evolution. In Figure 5, force and penetration depth plots are provided for three tests with 60° block orientation at different indentation rates up to a penetration depth of 25 mm. For this block orientation at an indentation rate of 0.01 mm/s the curve demonstrates combined brittle and crushing failure. The ice block at this slow indentation rate experienced repeated crushing events with an increasing trend of load but transitioned into ‘ductile’ failure at the end of the indentation. For the test performed at 0.25 mm/s, it can be observed that the failure process was dominated by crushing failure throughout the test. The crushing failure occurred with random crushing and irregular spalling failure events during the first millimeters of penetration depth, and as the load started to build up, irregular localized spalling events occurred with loads dropping to almost zero. For the test performed at 0.5 mm/s the curve exhibit evidence of crushing failure with spalling failure for the first half of the test and a combination of ductile and brittle failure can be observed at the end of the indentation.

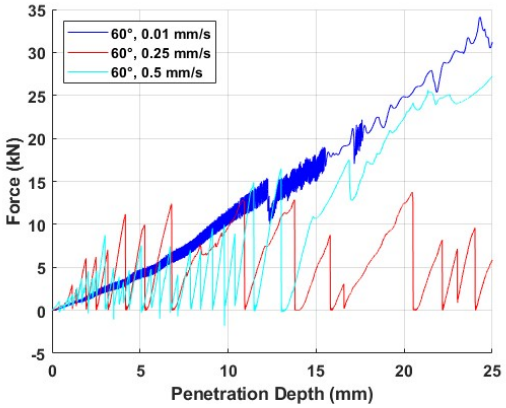

Figure 5. MTS load cell data for three different indentation rates: 0.01 mm/s (Test 06: blue); 0.25 mm/s (Test 03: red); 0.5 mm/s (Test 04: cyan)

The plot for nominal contact area and the experimental contact area as a function of penetration depth is given in Figure 6 for the three tests with indentation rates 0.01 mm/s, 0.25 mm/s, 0.5 mm/s. The tests investigated here were for ice blocks at 60° orientation. The nominal contact area evolution for ice block orientated at 60° orienatation, represented as the black line in Figure 6 (a), remained same for all rates. It can be seen from Figure 6 (a) for all the indentation rates, the experimental contact area increased with first few millimeters of penetration depth. The fast tests done at 0.25 mm/s and 0.5 mm/s showed a substantially lower contact area evolution with increasing penetration depth whereas the contact area increased for test performed at 0.01 mm/s. The amounts of fluctuations in the experimental contact area evolution appear to be influenced by the indentation rate. At slower rate of 0.01 mm/s, the experimental contact area appears to increase more than the nominal area with increasing penetration depth. At rates 0.25 mm/s and 0.5 mm/s, the experimental contact area demonstrated fluctuations indicating localized spalling events and loss of contact area due to crushing failure.

In Figure 6 (b), Contact Area Correction Factor (ψ_{AC}) is plotted as a function of the penetration depth for the three different rates. It can be seen from the figure that the correction factor for test at 0.01 mm/s the curve slightly fluctuates, yielding a correction factor value that varies between 0.9 and 1.2, indicating that the actual/experimental contact area of the block at this rate increases slightly more than therotical/nominal contact area. As a first order approximation, for slow indentation rates ψ_{AC} could be modelled as being an approximately constant value of 1.1. The actual contact area is greater than unity due to the damage enhanced creep nature of the local deformation processes for slow rate that causes the contact area to grow, which results in a contact area factor greater than 1. For the tests performed at fast indentation rates of 0.25 mm/s and 0.5 mm/s, it can be observed that at the onset of the indentation, the correction factor indicates the actual area is about twice as large as the nominal area for the first few milimeters of the indentation depth, with the actual area subsequently decreasing with increasing penetration depth. At higher indentation rates such as 0.25 mm/s and 0.5 mm/s, the failure process is dominated by localized spalling, and consequently the large spalls cause reduction in actual contact area as is reflected in the decreasing the correction factor with further increases in penetration depth. As a first order approximation, ψ_{AC} could be modelled as an exponential decay function that is capped at 1.75 for small penetration depths less than 2 mm, and which asymptotes to a relatively constant value of about 0.62 after about 10 mm penetration depth.

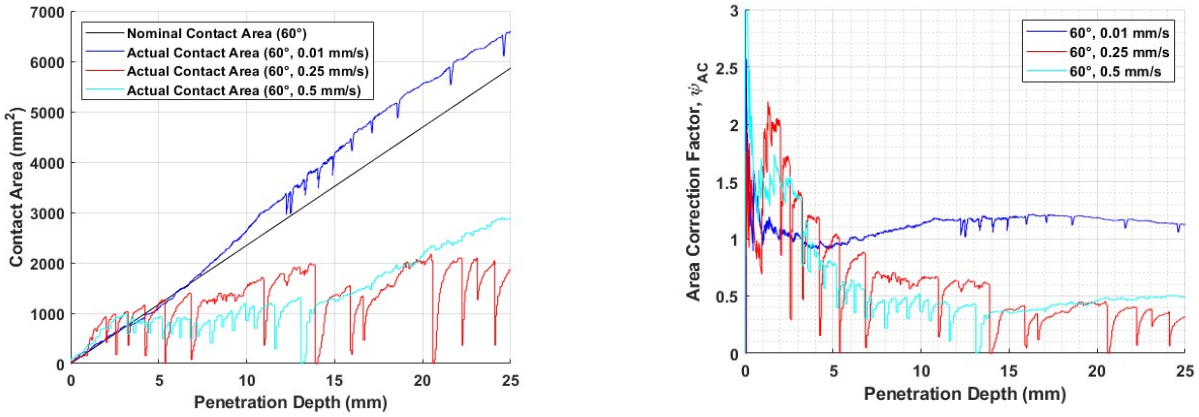

(a) (b)

Figure 6. (a) Contact area and (b) Area correction factor against penetration depth for three different indentation rates: 0.01 mm/s (Test 06: blue); 0.25 mm/s (Test 03: red); 0.5 mm/s (Test 04: cyan)

Images of the ice specimens shown in Figure 7 can be seen depicting the different failure modes during the slow and fast indentation rates. From Figure 7 (a) the image of the ice specimen show evidence of slow crushing with damaged enhanced creep which is characteristic of 'ductile' failure. Such failures exhibited an increase in the contact area at the interface between the ice block and the flat ice surface. For fast indentation rates, image in Figure 7 (b) show evidence of random fracture with extensive spalling that result in loss of contact area at the interface. These observation of differences for different indentation rate highlight the importance of the dependence of rate in the contact area evolution between ice blocks.

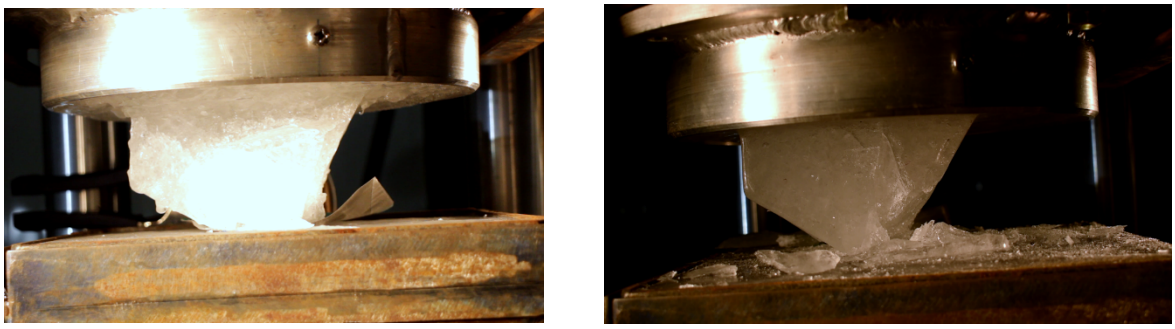

(a) (b)

Figure 7. Failure modes of the ice blocks at (a) slow indentation rate and (b) fast indentation rate.

To examine the trends in these results, the average forces, average area correction factors and average pressures were examined for all tests completed at 0.01 mm/s, 0.25 mm/s, and 0.5 mm/s for all orientation cases of 30°, 45° and 60°. Plot representing the average force observed for all indentation cases can be seen in Figure 8 (a). For the test completed at an orientation of 30° the average force was at largest value at 0.25 mm/s, with decreasing to the lowest value at 0.5 mm/s. For the test completed at 60° orientation, the maximum average force for all the cases was observed at 0.01 mm/s then the average force value trended down for the indentation rate at 0.25 mm/s before increasing for the test at 0.5 mm/s. For the test performed for the block orientation of

45° at 0.25 mm/s the average force value was recorded being close to the other tests completed at 0.25 mm/s.

Similarly, the average area correction factors and average pressures were examined for all tests completed at 0.01 mm/s, 0.25 mm/s, and 0.5 mm/s for all orientation cases of 30°, 45° and 60°. Plots representing the average area correction factors and average pressures observed for all indentation cases can be seen in Figure 8 (b) and 8 (c) respectively. From Figure 8 (b) similar trends are observed for the 30° block orientation case where the mean correction factor value dropped as the indentation rate increased from 0.25 mm/s to 0.5 mm/s/. For the 60° block orientation, the correction factor overpredicted the nominal area at 0.01 mm/s then declined and remained at a comparable level for both indentation rates of 0.25 mm/s and 0.5 mm/s. The average pressure trends from Figure 8 (c) exhibited a strong dependence on indentation rates. For both orientation angle of 30° and 60°, the average pressure follows an upward trend from the indentation rate of 0.25 mm/s to 0.5 mm/s.

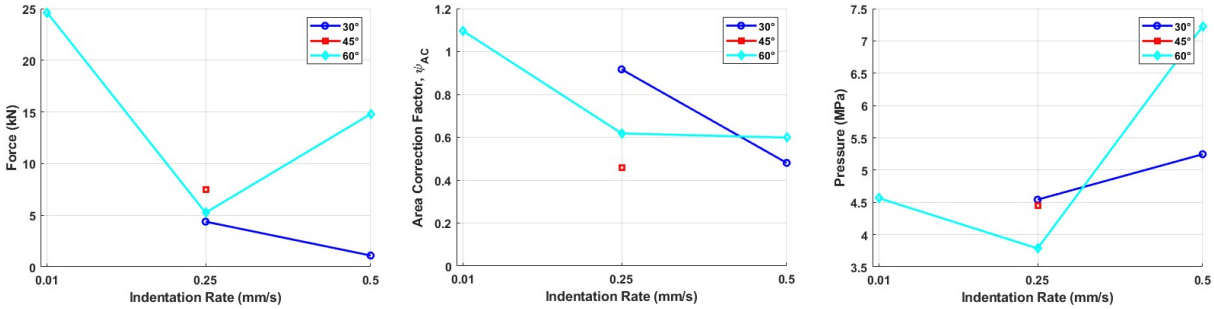

(a) (b) (c)

Figure 8. (a) Average MTS Load data (b) Average Area Correction Factor and (c) Average Pressure for different indentation rates.

Influence of Block Orientation

In order to investigate the effect of orientation of the ice block samples, tests were completed at three different block orientation angles. The angles were chosen as 30°, 45° and 60°. The post-test images of the ice samples at different orientation angles are given in Figure 9. These tests investigated here were performed at an indentation rate of 0.25 mm/s. From the post-test images below for all the different block orientation angles, crushing failure and localized spalling events are most prominent. The plot of force against penetration depth in Figure 10 (a) further verifies that the ice samples experienced random failure with crushing and spalling throughout the tests for all orientation angles. From Figure 10 (b), the area correction factor curves for all three orientation angles are observed to demonstrate similar trends at the indentation rate of 0.25 mm/s. The area correction factors for these tests are observed to decrease with increasing penetration depth. Irregular spalling events throughout these tests is considered to be the main contributor to the observed decrease in the area correction factor for all cases of orientation angles.

(a) (b) (c)

Figure 9. Post-test images of ice samples with an orientation angle of (a) 30° (b) 45° (c) 60°.

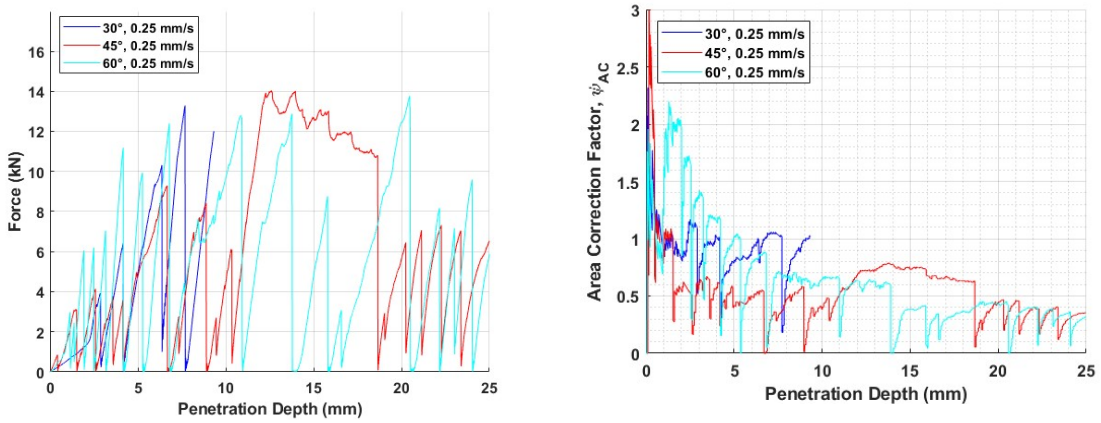

(a) (b)

Figure 10. (a) MTS load cell data and (b) Area correction factor against penetration depth for three different orientation angles: 30° (Test 01: blue); 45° (Test 05: red); 60° (Test 03: cyan)

The plots of average force, average area correction factor and average pressure are provided in Figure 11 for the three different orientation angles. From Figure 11 (a) the highest magnitude of average force can be observed for 0.01 mm/s case at 60° orientation angle. The data point for the 0.01 mm/s case is too few data to draw meaningful conclusions; therefore, additional data collection at this indentation rate would be beneficial to make significant evaluation and is suggested as a future recommendation. For the 0.25 mm/s the ice samples showed slightly higher average forces in 45° orientation as compared to 30° and 60° orientation angles. For the 0.50 mm/s case the ice sample showed a higher force in 60° orientation angle than the 30° angle. Plots representing the average area correction factors and average pressures observed for all orientation angle cases can be seen in Figure 11 (b) and 11 (c) respectively. From the plots it is evident that no significant difference between the test cases at 45° and 30°- 60°.

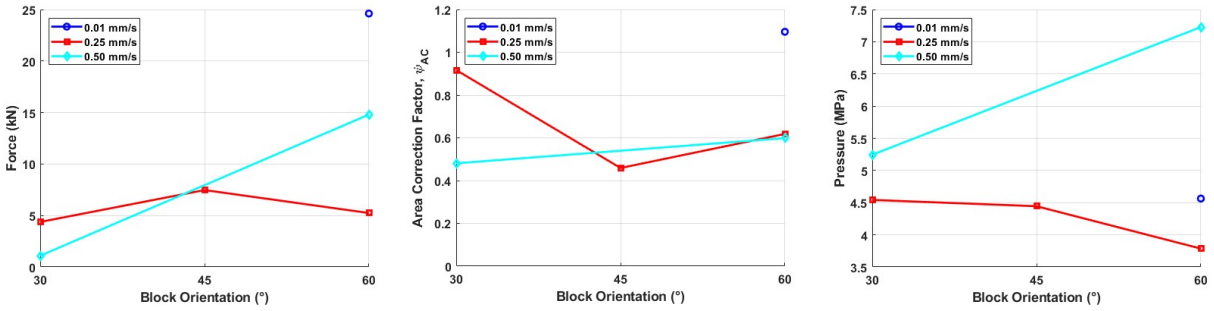

(a) (b) (c)

Figure 11. (a) Average MTS Load data (b) Average Area Correction Factor and (c) Average Pressure for different orientation angles.

The Table 2 below provides a summary of the average correction factor values for all tests completed at 0.01 mm/s, 0.25 mm/s, and 0.5 mm/s for all orientation cases of 30°, 45° and 60° angles.

Table 2. Average area correction factor values for all test cases.

Test No.	Indentation Rate (mm/s)	Orientation (°)	Contact area correction factor, ψ_{AC}
01	0.25	30	0.92
02	0.5	30	0.48
03	0.25	60	0.62
04	0.5	60	0.60
05	0.25	45	0.46
06	0.01	60	1.10

Based on the data provided in the Table 2, the average contact area factor (ψ_{AC}) for fast interaction rates and slow interaction rates can be approximated as 0.62 (62% of the nominal/theoretical contact area) and 1.10 (110% of the nominal/theoretical contact area) respectively. The Table 3 below provides the mean and the standard deviation of the area correction factor for the collective fast tests (0.25 mm/s and 0.5 mm/s) and the slow test (0.01 mm/s).

Table 3. Mean and Standard Deviation of area correction factor for fast vs. slow test.

Test Type	Mean ψ_{AC}	Standard Deviation
Fast	0.62	0.18
Slow	1.10	0.11

CONCLUSIONS AND RECOMMENDATIONS

In this paper, the influence of indentation rate and ice block geometry on contact area evolution under compressive loading were investigated. An analysis of force, contact area and contact pressure data collected during a set of experiments including three indentation rates and three block orientation angles has been conducted.

According to this analysis, it has been deduced that indentation rates during the ice block-block interaction was observed to strongly influence the failure mechanism and contribute to the variability in measured force, pressures and contact area development. The failure mode was observed to shift from random fracture for fast rates to damage enhanced creep for slow. Results showed that the average area correction factors varied from 0.48 to 1.10. Lowest area correction factors were measured at high indentation rates of 0.25mm/s and 0.5 mm/s that corresponded closely with the loss of contact area due to crushed/extruded ice during the indentation. Peak area correction factor was measured at slow indentation rate of 0.01 mm/s that corresponded increase of contact area due to slow crushing and "ductile" failure during the indentation.

The block geometry of the ice specimens showed insignificant differences in loading patterns, average force, pressure and contact area evolution. Average area correction factors measured for the different orientation angles is observed to have no substantial difference. However, additional data are required in order to solidify this assessment, since only small numbers of tests were possible as a result of lack of cold room availability.

In summary, the crushing behaviors and the contact area evolution were observed to depend largely on the indentation rate, however, it appeared to be less sensitive to the orientation of the ice samples. From the analysis, the contact area correction factor is approximated to be 0.62 for fast rate and 1.10 for the slow rate. These approximated values for the contact area factors can be used in similar type of experiments in the future to the estimate contact area, pressure and freeze-bond strength during freeze-bonding process at the interface between two ice rubble blocks. Further work to gather additional repeats and evaluate these effects over a broader range of conditions is recommended. To better assess how observed results scale to field conditions, additional experiments at medium and large-scales are recommended. While the contact area ratio was observed to not be sensitive to orientation, additional experiments to verify this is also the case for multiple axes of rotation for the ice block specimens are recommended. Such work would provide better insight and greater confidence in modeling the evolution of block-block contact area that occur internally within ice ridges during natural sea ice deformation processes, as well as during interactions with ships and structures.

ACKNOWLEDGEMENT

The authors would like to acknowledge the following people: Mr. Craig Mitchell and Mr. Matthew Curtis for their assistance during the laboratory experiments. The authors also gratefully acknowledge funding from Hibernia Management and Development Company, Ltd. (HMDC), Terra Nova Development (Suncor Energy Inc.), and the Natural Sciences and Engineering Research Council of Canada (NSERC) for this work.

REFERENCES

Afzali, S., Taylor, R., Bailey, E., Sarracino, R., and Boroojerdi, M. T. 2021. Investigation of the Effect of Block Size, Shape, and Freeze Bond Strength on Flexural Failure of Freshwater Ice Rubble Using the Discrete Element Method." ASME. *Journal of Offshore Mechanics and Arctic Eng*ineering, 143(5), pp.1-7.

Bailey, E, Taylor, R, & Croasdale, KR., 2015. Mechanics of Ice Rubble Over Multiple Scales. *Proceedings of the ASME 2015 34th International Conference on Ocean, Offshore and Arctic Engineering*, pp. 1-2.

Heinonen, J., 2004. *Constitutive modeling of ice rubble in first-year ridge keel*. VTT Technical Research Centre of Finland, pp. 19-23.

Jensen, A., Høyland, K. V., & Evers, K. U., 2000. SCALING AND MEASUREMENT OF ICE RUBBLE PROPERTIES IN LABORATORY TESTS. *In Proceedings of the 15th International Symposium on Ice (IAHR)*, pp. 105-112.

Palmer, A. & Croasdale, KR., 2013. *Arctic offshore engineering*. World Scientific.